

Transcriptional landscape of human microglia reveals robust gene expression signatures that implicates age, sex and *APOE*-related immunometabolic pathway perturbations

Tulsi Patel

Mayo Clinic Florida

Troy Carnwath

Mayo Clinic Florida

Xue Wang

Mayo Clinic

Mariet Allen

Mayo Clinic Florida

Sarah Lincoln

Mayo Clinic Florida

Laura Lewis-Tuffin

Mayo Clinic Florida

Zachary Quicksall

Mayo Clinic Florida

Shu Lin

Mayo Clinic Florida

Frederick Tutor-New

Mayo Clinic Florida

Charlotte Ho

Mayo Clinic Florida <https://orcid.org/0000-0002-9135-1652>

Yuhao Min

Mayo Clinic Florida

Kimberly Malphrus

Mayo Clinic

Thuy Nguyen

Mayo Clinic Florida

Elizabeth Martin

Mayo Clinic Florida

Cesar Garcia

Mayo Clinic Florida

Rawan Alkharboosh

Mayo Clinic Florida

Sanjeet Grewal

Mayo Clinic Florida

Kaisorn Chaichana

Mayo Clinic Florida

Robert Wharen

Mayo Clinic Florida

Hugo Guerrero-Cazares

Mayo Clinic Florida <https://orcid.org/0000-0003-1307-719X>

Alfredo Quinones-Hinojosa

Mayo Clinic Florida <https://orcid.org/0000-0003-4262-5968>

Nilufer Ertekin-Taner (✉ Taner.Nilufer@mayo.edu)

Mayo Clinic Florida

Article

Keywords: Alzheimer's disease, neurodegeneration, APOE

Posted Date: June 7th, 2021

DOI: <https://doi.org/10.21203/rs.3.rs-523348/v1>

License:   This work is licensed under a Creative Commons Attribution 4.0 International License.

[Read Full License](#)

Abstract

Microglia have fundamental roles in health and disease, however effects of age, sex and genetic factors on human microglia have not been fully explored. We applied bulk and single cell approaches to comprehensively characterize human microglia transcriptomes and their associations with age, sex and *APOE*. We identified a novel microglial signature, characterized its expression in bulk data from 1,306 brain samples across 6 regions and in single cell microglia transcriptome. We discovered microglial co-expression network modules associated with age, sex and *APOE-ε4* that are enriched for lipid and carbohydrate metabolism genes. Integrated analyses of modules with single cell transcriptomes revealed significant overlap between age-associated module genes and both pro-inflammatory and disease-associated microglial clusters. These modules and clusters harbor known neurodegenerative disease genes including *APOE*, *PLCG2* and *BIN1*. These data represent a well-characterized human microglial transcriptome resource; and highlight age, sex and *APOE*-related microglial immunometabolism perturbations with potential relevance in neurodegeneration.

Introduction

Microglia are the resident macrophages of the central nervous system (CNS), responsible for clearance of cellular debris and pathological protein aggregates. In the healthy brain they exist in a resting state and can be induced to a reactive state in response to changes in the CNS microenvironment, such as inflammation and neuronal damage¹. They are fundamental to maintaining brain homeostasis during development, aging and disease, therefore microglial dysfunction could ultimately lead to neurodegeneration². Microglia are integral to the pathophysiology of neurodegenerative diseases, including Alzheimer's disease (AD) and multiple sclerosis, with chronic inflammation implicated as a contributing factor³⁻⁵.

Fresh human brain tissue studies are imperative to the characterization of the microglial transcriptome in health and disease; however, accessibility is limited. Although single nuclei studies using frozen tissue provide an easier alternative, recent studies have demonstrated limitations in detecting substantial populations of less abundant cell types^{6,7}. Additionally, it was recently reported that many microglial activation genes are expressed in the cytosol and therefore are likely to be missed by single nuclei RNA sequencing (snRNAseq)⁸. Recent single cell studies aiming to characterize microglial gene expression using fresh tissue have highlighted the heterogeneity in microglial phenotypes⁹⁻¹¹. This has revealed that phenotypic changes are not binary but rather a spectrum of states in which microglia can simultaneously co-exist during transition from resting to more reactive states. Additionally, these different subsets could have specialized functions in brain homeostasis and dysfunction. Thus, it is increasingly important to characterize these heterogeneous subpopulations to understand their roles in health and disease. This could also help facilitate the design of novel therapeutic approaches to target specific subpopulations of cells and modulate their activity².

Microglial expression has been shown to be affected by aging^{12,13}, however few studies have investigated the effects of sex and genetic factors on human microglia. Sex differences in microglia have been previously reported in mice, with females being predisposed to harboring more activated microglia than males¹⁴⁻¹⁶. *APOE*, a lipoprotein of which the $\epsilon 4$ allele (*APOE- $\epsilon 4$*) is a major risk factor for AD and also implicated in other neurodegenerative diseases¹⁷, is upregulated in disease-associated microglia (DAM) in mice and humans, but downregulated in astrocyte and oligodendrocyte subpopulations^{4,6,18,19}. In microglia and neurons, *APOE* interacts with LDL receptors to facilitate endocytosis of cholesterol and phospholipids and modulate lipid homeostasis in the brain²⁰. Such studies provide growing support for cell type-specific functions of *APOE*, however, its effects on microglia remain to be fully elucidated. Thereby identifying age, sex and *APOE*-associated pathways in microglia will provide greater insight into the functions of specific microglial subsets in relation to these risk factors. Inter-individual variability and diversity in functional states makes targeting specific microglial subsets in disease challenging for modulating these cells². Identifying the mechanisms regulating microglial homeostasis and activation can allow us to manipulate these cells for therapeutic purposes.

In this study, we leveraged both bulk and single cell approaches to provide a comprehensive characterization of the adult human microglial transcriptome. We obtained fresh intraoperative neurosurgical brain tissue and isolated an enriched population of microglial cells to investigate transcriptional changes associated with age, sex and *APOE- $\epsilon 4$* in bulk microglia and further explored these in single microglial cells. Our findings support age-, sex- and *APOE*-related microglial transcriptome changes involving lipid and carbohydrate metabolic pathways and implicate microglial immunometabolism perturbations relevant to neurodegenerative diseases.

Results

To uncover microglial transcriptional profiles and their associations with age, sex and *APOE*, we performed microglial cell-type specific and single cell RNA sequencing (scRNAseq) studies in fresh human brain tissue. We isolated CD11b⁺ microglial cell populations from neurosurgical tissue unaffected by the primary disease process (**Supplementary Figure S1**) and obtained from 19 human donors for bulk microglia RNA sequencing (RNAseq) (Fig. 1a). Subsets of these and additional samples also underwent 10x scRNAseq (n = 5) and bulk tissue RNAseq (n = 9) (**Supplementary Table S1**). Validation of sorted microglia using qPCR showed the expected *CD11b⁺/CD45^{intermediate}/P2RY12⁺* microglial signature² with no expression of other cell type markers, indicating that we isolated a highly enriched microglial population (**Supplementary Figure S2**).

Identification of a core human microglial transcriptional signature

To define a core human microglial signature, we calculated log₂ fold change and q-values of differential expression for each gene between bulk microglia RNAseq data in our study and bulk brain RNAseq data from 7 AMP-AD datasets provided by Mayo Clinic²⁴, Mount Sinai Brain Bank²⁵ and Rush University

Religious Orders Study and Memory and Aging Project (ROS-MAP)²⁶ representing 6 brain regions from 515 human samples. Using a cutoff of 4-fold greater expression in our bulk microglia and a q-value threshold of 0.05, we identified 1,971 genes (**Supplementary Tables S2-4**). These genes were expressed at significantly greater levels in our bulk microglial transcriptome data in comparison to each of the bulk brain transcriptome datasets. Therefore, we considered these 1,971 genes as the core microglial signature in our dataset. This signature comprises several known marker genes, with 12.7% of the genes being BRETIGEA³³ microglial genes, suggesting that it also likely harbors novel microglial markers of interest. GO enrichment using MSigDB showed that this signature was enriched for genes involved in immune-related and inflammatory response pathways as would be expected, and leukocyte mediated immunity (Fig. 1b).

To determine the ability of bulk brain tissue data to capture microglial genes, we assessed the expression levels of our microglial signature genes in each of the 7 AMP-AD bulk brain RNAseq datasets. Of the 1,971 microglial signature genes in our study, 37–47% were captured in these bulk brain datasets, with least numbers captured in MSSM superior temporal gyrus and most numbers in Mayo Clinic cerebellum (**Supplementary Figure S3a-b**). Our microglial signature genes comprised 3.6–4.5% of the expressed bulk brain transcriptome, consistent with prior estimations^{6,34}. We next compared bulk microglia RNAseq transcript levels to that obtained from bulk tissue RNAseq of neurosurgical fresh brain tissue samples. Bulk fresh brain tissue does not capture all microglial marker genes, as demonstrated by the low correlation between bulk tissue and bulk microglia data (**Supplementary Figure S3c**). This reiterates the need for complementary single cell type data to deconvolute cell type specific expression. We provide the list of microglial signature genes that are also expressed at high levels in bulk brain tissue data (**Supplementary Table S5**), which can serve as a validated resource for microglial signature gene markers in bulk RNAseq datasets.

To determine how the microglial signature in this study compared to previously published signatures, we performed hypergeometric tests of overrepresentation with Galatro, et al.¹², Gosselin, et al.³⁵ and Olah, et al.¹³ studies. Significant overlap was observed across all datasets, with 350 genes common to all datasets (Fig. 1c-d, **Supplementary Table S4**). This comprised several established microglial marker genes, including *P2RY12*, *TMEM119* and *CX3CR1*. The most significant overlap was shared with Gosselin, et al.³⁵ signature [OR = 19.6 (17.0-Inf) p = 3.8E-261], where 49.7% of their genes were also present in our signature, and 22% of ours in their signature. Gosselin, et al.³⁵ samples were also obtained from neurosurgical tissue resections like our cohort; and are unlike Galatro, et al.¹² and Olah, et al.¹³ samples that were harvested during autopsy. Although there appears to be a common set of microglial genes consistent across signatures, each also harbors many unique genes, which could be due to study or individual specific differences.

Transcriptional profiling of microglia discovers co-expression networks and implicates lipid and carbohydrate metabolism pathways associated with age, sex and *APOE*

We generated gene co-expression networks using WGCNA³⁰ to reduce number of tests and increase power to detect genetic associations with age, sex and *APOE*. We identified 7 modules with significant associations (Fig. 2; **Supplementary Figure S4; Supplementary Table S6**). Modules ME14 and ME34 associated with age, however, in opposite directions. ME14 was enriched for genes involved in the lipid localization pathway that were upregulated with age ($R = 0.50$, $p = 0.03$) (Fig. 2a-c). ME34, enriched for DNA endoreduplication genes, had negative association with both age ($R = -0.55$, $p = 0.01$) and *APOE-ε4* ($R = -0.50$, $p = 0.03$), indicating that microglial transcripts involved in this pathway are downregulated with aging and in *APOE-ε4* carriers (Fig. 2a). Several other modules also associated with *APOE-ε4*, in either direction. The only module associated with sex was ME26, which was downregulated in females ($R = -0.54$, $p = 0.02$), and enriched for genes involved in cholesterol absorption and lipid digestion. This module also had the most significant association with *APOE*, in the positive direction with presence of *APOE-ε4* ($R = 0.66$, $p = 0.002$) (Fig. 2a,b,e). Of the *APOE* associated modules, ME23 had the second most significant association ($R = -0.61$, $p = 0.006$) and was enriched for carbohydrate metabolism genes (Fig. 2a,b,d). Given recent discoveries in microglial immunometabolism³⁶⁻³⁹, we focused on ME14, ME23 and ME26 that are enriched for lipid and carbohydrate metabolism genes.

ME14 co-expression network (Fig. 2c) hub genes *NPC2*, *MSR1* and *PLAU* are also microglial signature genes in our study and known to be involved in microglial functions^{40-44, 45}. Several disease-associated microglial (DAM) markers are also present in this network, including *CD9*, *ARAP2* and *MYO1E*^{4,46,47} that are increased with aging, implicating activated microglial lipid localization pathways in aging (Fig. 2f). Several genes in this module were also previously linked to neurodegeneration, including *MYO1E*^{48,49}, *CTSL*⁵⁰ and *UNC5B*^{51,52}.

Our microglial signature (**Supplementary Tables S2-S4**) had significant overrepresentation of the age-associated ME14 genes (**Supplementary Table S6**) (OR = 1.55 [95% CI = 1.23-INF], $p = 0.001$), highlighting age-related increases in microglial signature genes. Galatro, et al.¹² and Olah, et al.¹³ also reported age-related microglial signatures. Comparison of ME14 genes revealed significant overlap with Olah, et al.¹³ (OR = 1.34 [95% CI = 1.05-INF] $p = 0.03$), but not with Galatro, et al.¹² microglial aging signature genes.

ME26 cholesterol metabolism pathway genes exhibited reduced expression in males and were elevated in *APOE-ε4* carriers (Fig. 2a,b). This module contains known microglial genes *LDLR*, *CD36* and *CRIP1* (Fig. 2e,f). Assessment of individual ME26 network genes revealed *C17orf49*, *RP11-589P10.7* and *MIR497HG* to be the only microglial signature genes in this network to be associated with both sex and *APOE* (Fig. 2e). Other microglial signature genes in ME26 associated with only sex or only *APOE*, suggesting that these traits may have independent effects on expression of some microglial genes. Several *APOE*-associated genes in ME26 were previously implicated in AD, including *CASP7*^{53,54} and *LDLR*^{55,56} (Fig. 2f).

Carbohydrate metabolism gene enriched module ME23 is downregulated in *APOE-ε4* carriers (Fig. 2a,b,d). AD risk genes *BIN1*⁵⁷ and *PLCG2*⁵⁸ are present in this network, which have both been implicated in

microglial dysfunction in neurodegeneration (Fig. 2d).

Single cell transcriptome reveals specific subtypes of microglia

To uncover distinct microglial subtypes, a subset of sorted microglial samples from neurosurgical brain tissue underwent single cell expression profiling. We obtained 26,558 cells from 5 unique individuals, including one individual who underwent epilepsy surgery and had samples from two brain regions (**Supplementary Table S1**). Analysis of the scRNAseq data from these samples revealed 13 distinct cell clusters which were annotated using established microglial marker genes from the literature^{4,6,9-11,47,59,60} (Fig. 3a, **Supplementary Table S7**). Myeloid markers (*AIF1*, *PTPRC*, *C1QA*) were detected in all clusters except cluster 12 which expressed oligodendrocyte markers (*PLP1*, *MBP*, *MOBP*). Cluster 9 expressed macrophage-specific markers (*VCAN*, *FCN1*, *CRIP1*, *S100A8*). These two clusters comprised only < 3% of all cells, indicating that our sorted samples represent a very pure microglial population. Each myeloid cluster had cellular contributions from all samples, albeit with some variability in their proportions, likely due to intrinsic differences between individuals (Fig. 3b, **Supplementary Table S8**). Samples from two brain regions obtained from the same individual undergoing epilepsy surgery revealed similar cellular contributions in each cluster (**Supplementary Table S8**). For these samples, the most marked difference was observed for macrophages (cluster 9) and homeostatic microglia (cluster 2), which had greater contributions from the mesiotemporal and anterior temporal regions, respectively. This could be due to the proximity of the mesiotemporal sample to the disease-affected region.

We characterized the microglial clusters by their expression of established microglial subtype markers (Fig. 3c, **Supplementary Figure S5**) and their most significant marker genes (**Supplementary Figure S6**). Homeostatic (*TMEM119*, *P2RY12*, *CX3CR1*)^{10,11,47,60}, pro-inflammatory (*CCL2*, *CCL4*, *EGR2*)^{10,11} and DAM markers (*APOE*, *C1QA*, *C1QB*)^{4,9,11,18} were observed in clusters 2, 1/6 and 10, respectively. Cluster marker genes are defined as those expressed in at least 70% of the cells in the cluster with log fold change > 0.6 and $q < 0.05$ in comparison to all other clusters. Expression levels of the top marker genes per cluster are shown (Fig. 3c; **Supplementary Figure S6; Supplementary Table S9**). Most of these markers are distinct to a single cluster, although some clusters appeared to have similarities in their marker expressions. To define the proximity of their transcriptional profiles, we performed hierarchical clustering of the microglial clusters (Fig. 3d). We determined that the homeostatic microglia cluster 2 was transcriptionally closest to clusters 7 and 11, which may represent subtypes of homeostatic microglia. Clusters 1 and 6 both expressed chemokines *CCL2* and *CCL4* representative of pro-inflammatory microglia, however cluster 6 was more closely related to DAM, whereas cluster 1 represented a more distinct microglial signature. Cluster 6 highly expressed interferon-related marker *IFITM3* and *ISG15*, also observed in a cluster by Olah et al (2020)⁹, which they defined as an interferon response-enriched subset. These findings highlight different transcriptional profiles for the two pro-inflammatory microglial clusters that may represent distinct activated microglia subtypes. Cluster 3 highly expressed heat shock protein *HSPA1A*, an immediate early gene⁶¹ reportedly involved in antigen processing⁶² and exhibiting decreased gene expression in multiple sclerosis patients^{63,64}. These proteins are involved in the stress response. Several were upregulated in this cluster, suggesting that this cluster may represent cells that underwent

dissociation-induced stress¹¹. Six of the clusters could not be annotated based on existing cell type markers. Clusters 5/8 and 0/4 were transcriptionally closest to one another (Fig. 3d). Cluster 5 has distinct expression of immunoreactive marker *CD163*, which was not observed in other subsets except macrophages. Several *HLA* genes are also highly expressed in this cluster. Our findings highlight transcriptional profiles for known microglial clusters, describe the transcriptional proximity of these clusters and suggest that less well-defined clusters could potentially represent novel or intermediate transcriptional states of microglia.

To determine whether the bulk microglial co-expression networks (Fig. 2a,c-e, **Supplementary Figure S4**) were representative of microglial subtypes, we performed enrichment analyses of the module genes within the myeloid clusters with sufficient cell numbers (Fig. 3e). Age-associated co-expression network ME14, implicated in lipid metabolism, was significantly enriched in pro-inflammatory (cluster 6) and DAM (cluster 10) clusters. Genes within module 28, which was significantly upregulated with *APOE-ε4*, had statistically significant enrichment in all clusters except cluster 7. There was no statistically significant enrichment for any of the other microglial modules that had significant age, sex or *APOE* associations, suggesting that these factors may have ubiquitous effects on most microglial subtypes. Some of the remaining microglial co-expression networks had distinct patterns of cluster enrichment (**Supplementary Figure S7**), suggesting that some but not all networks could be representative of distinct microglial subtypes.

Discussion

Given their critical functions in maintaining homeostasis in the central nervous system (CNS) in health and their multifaceted roles during neurological diseases^{2,3}, understanding the biology of microglia and characterizing microglial subtypes is essential. Large scale studies in bulk brain tissue²⁴⁻²⁶ have been instrumental in establishing transcriptional profiles in health and neurodegenerative diseases. Although these studies yielded information on brain expression signatures and uncovered perturbed pathways and molecules implicated in Alzheimer's disease and other neurological disorders⁶⁵⁻⁶⁸, they are limited in their ability to provide cell-type specific transcriptional outcomes, especially for less abundant CNS cells such as microglia³⁴. Analytic deconvolution approaches began to leverage these bulk tissue transcriptome datasets to estimate cell-type specific expression profiles^{33,34}, but the accuracy of these methods relies on the availability of high quality single cell-type datasets. Such microglia-specific transcriptome datasets are gradually emerging^{9,12,13,35}, although the numbers of unique samples assessed remain limited given the arduous nature of collecting fresh human brain tissue. Additionally, comparative assessment of bulk brain vs. single cell-type bulk microglia vs. single-cell microglia studies are still rare^{9,69,70}. To our knowledge there are no studies that evaluate human microglial transcriptome using all three approaches, as in our study. Further, investigations on effects of genetic and other factors on microglial transcriptional signatures in humans is likewise sparse, with the exception of age-related effects assessed in a few studies^{12,13,35}. Finally, unlike in bulk tissue studies^{33,65-68}, microglia-specific co-expression networks, their molecular signatures and functional implications have not been evaluated.

In this study, we sought to overcome these knowledge gaps by characterizing the transcriptome of sorted bulk and single-cell microglial populations isolated from fresh human brain tissue. We identified a robust microglial signature comprising 1,971 genes enriched for immune-related functions. These signature genes were selected due to their consistently higher expression levels in our sorted bulk microglial transcriptome in comparison to 7 different bulk brain tissue datasets from 6 different regions²⁴⁻²⁶. We also compared sorted bulk microglia to bulk fresh brain tissue and identified transcripts that are expressed in both. The microglial signature genes that are also reliably detected in bulk brain tissue represent a validated list of microglial markers that can be utilized in bulk brain tissue transcriptome analytic deconvolution studies^{33,34}.

Our microglial signature significantly overlapped with other signatures from bulk microglia previously reported by Galatro, et al.¹², Gosselin, et al.³⁵ and Olah et al.¹³, implicating a core set of genes consistently expressed in this cell type. However, there were additional genes unique to each signature, likely to be driven by factors such as patient demographics or study differences. Galatro, et al.¹² and Olah et al.¹³ both also reported age-related microglial expression signatures. We found significant overlap of our age-associated microglial gene expression module ME14 genes with the latter, which was also enriched for our microglial signature. This indicates that bulk microglial profiles can effectively capture genes affected by aging in microglia.

We leveraged the co-expression network structure of sorted bulk microglia to further explore whether microglial subsets were associated with age, sex or *APOE-ε4*. To our knowledge sex-differences in microglial transcriptome were previously studied only in mice¹⁴⁻¹⁶, however *APOE* genotype-specific microglial interactions with amyloid plaques have been previously observed in mice^{15,71} and humans⁷². We identified two network modules associated with age, one with sex and six with *APOE-ε4*. We observed that two modules, ME14 that is positively associated with increased age; and ME26 that is positively associated with both *APOE-ε4* and female sex, were both enriched for lipid metabolism biological terms³⁶⁻³⁸. Module ME14 included genes involved in lipid localization and storage pathways (*PLIN2*, *IL6*, *LPL*, *MSR1*, *ENPP1*, *PPARG*, *PTPN2*, *SOAT1*, *IKBKE*) and ME26 had lipid digestion/cholesterol transport pathway genes (*CD36*, *LDLR*). Both modules harbored known microglial genes (*LDLR*, *CD36*, *CRIP1*, *NPC2*, *MSR1*, *PLAU*) and those that are included in our microglial signature (*PLIN2*, *IL6*, *MSR1*, *SOAT1*, *IKBKE*, *NPC2*, *PLAU*).

Comparing the sorted bulk microglial network modules to scRNAseq microglial clusters, we determined that ME14 genes were significantly over-represented in pro-inflammatory cluster 6 and disease-associated microglia (DAM) cluster 10. In our study, DAM cluster 10 included *APOE*, *APOC1*, *ASAH1* and *CTSD*. Of these *APOE*^{17,37,73}, *APOC1* and *ASAH1*⁷⁴ are involved in lipid metabolism and neurodegenerative diseases. *APOE*^{4,5,18}, *APOC1*¹⁸ and *CTSD*⁴ were also signature genes in mouse models of neurodegenerative diseases^{4,5} or aging¹⁸. Our pro-inflammatory cluster 6 also included genes associated with mice microglial neurodegenerative (*FTH1*⁴) or aging signatures (*CCL4*¹⁸), as well as *IFITM3*³⁸, *GOLGA4*³⁸, previously shown to be upregulated in aging lipid droplet accumulating microglia³⁸.

Our findings that integrate human sorted bulk RNAseq and scRNAseq data, support a model where aging human microglia transition to a pro-inflammatory and disease-associated transcriptional profile which is also associated with perturbations in lipid metabolism in these cells.

There is increasing evidence that tightly controlled lipid metabolism is essential to the functions of microglia during development and homeostatic functions of adulthood and may be disrupted in aging and disease^{36,37}. The complex interactions between microglial lipid metabolism and its cellular functions rely on lipid sensing by microglial receptors such as CD36 and TREM2 and uptake of lipids, including LDL and APOE^{36,37}. These interactions are necessary for microglia to become activated and perform functions including phagocytosis of myelin⁷⁵ and misfolded proteins like amyloid β ⁷⁶, cytokine release, migration and proliferation^{36,39}. Studies primarily focused on *in vitro* and animal models suggest disruption of the microglial immunometabolism and assumption of a pro-inflammatory phenotype with aging^{18,38,77,78} and diseases including multiple sclerosis (MS) and Alzheimer's disease^{4,5,79}. Interestingly, microglial lipid droplet accumulation has been demonstrated under all these conditions^{36-38,75} and lipid droplet accumulating microglia in aging mice were shown to have a unique transcriptional state³⁸. Our findings in sorted cells from fresh human brain tissue provide transcriptional evidence for immunometabolism changes and pro-inflammatory phenotype with microglial aging, thereby contributing essential complementary data from humans for this cell type.

Besides module ME14, we determined that ME26 is also enriched for lipid metabolism genes. ME26 module expression is higher in both *APOE- ϵ 4* and female sex, however we note that in our sorted bulk microglia RNAseq samples, there were no male *APOE- ϵ 4* carriers. Therefore, the distinct influence of sex and *APOE* on the expression of this module remains to be established. *APOE- ϵ 4*, a major risk factor for Alzheimer's disease, has the lowest lipid binding efficiency compared with other *APOE* isoforms³⁶. Increased cholesterol accumulation has been reported in both iPSC-driven astrocytes from *APOE- ϵ 4* carriers⁸⁰ and also in *ApoE*-deficient microglia⁷⁵. These findings collectively support a role for *APOE- ϵ 4* associated microglial transcriptional changes and disrupted cholesterol metabolism. Using our sorted microglia RNAseq data, we identified five additional modules that associate with *APOE- ϵ 4*, one in a positive direction (ME28) and four negatively (ME4, ME23, ME34, ME36). Of these, module ME23 had the second most significant *APOE- ϵ 4* association after ME26. Interestingly, ME23 was enriched for carbohydrate metabolism biological processes, which are also tightly regulated in microglia³⁹. Module ME23 harbors known AD risk genes *BIN1* and *PLCG2*, where the latter is a microglial gene that modulates signaling through *TREM2*⁸¹ and also a hub gene in this module. ME23 genes *BIN1*, *JUN* and *TGFBR2* were found to be reduced in a mouse microglial neurodegenerative phenotype gene signature⁵. These findings further demonstrate the consistency of our human microglial data with that from mouse models and supports perturbed microglial immunometabolism as a potential pathogenic mechanism in neurodegeneration.

In addition to analyzing gene expression modules from sorted bulk microglia, we also identified microglial clusters from sorted microglial scRNAseq data. To our knowledge, there are only two prior

publications of scRNAseq characterizations on human microglia^{9,10}. Masuda et al.¹⁰ analyzed 1,602 microglia isolated from 5 control and 5 MS patient brains, compared their findings to those from mice demonstrating clusters that are common and others that are species-specific. Olah et al. assessed 16,242 microglia from 17 individuals and characterized subclusters of microglia from patients with mild cognitive impairment, AD and epilepsy⁹. Our scRNAseq dataset is from 5 unique individuals comprising 26,558 cells, 99.98% of which have myeloid markers. We identified microglial clusters that share characteristics of those previously reported in mice⁴ and humans^{9,72}, such as DAM. We also uncovered clusters that could not be readily annotated, including cluster 7, characterized by high microglial expression of the astrocytic *SLC1A3*. Microglial expression of *SLC1A3* was previously shown to occur in mice and humans especially in disease states⁸²⁻⁸⁴. We also leveraged these scRNAseq data to further characterize the sorted bulk microglial expression modules. Hence our microglial scRNAseq data contribute further to the emerging single cell landscape of this cell type.

We acknowledge that our study has several limitations, primarily owing to the difficulty in obtaining high quality neurosurgical brain tissue, which leads to limited sample size and variability in tissue, diagnoses and patient demographics. Even though we have utilized control tissue surgically separated from disease tissue, the samples are from epilepsy and various brain tumor patients representing multiple diagnoses. Although we isolated microglia using an approach which should minimize activation, we cannot definitively rule out stress-induced transcriptomic changes during isolation. Despite these caveats, we could identify microglial co-expression modules and subclusters with multiple features that are consistent with prior publications from model systems^{4,5,18,38}. Our scRNAseq clusters have contributions from both tumor and epilepsy samples, suggesting that our findings are unlikely to be driven by any one diagnoses.

In summary, our study on sorted bulk microglia RNAseq and scRNAseq from fresh brain tissue yield several key findings. We identify a microglial gene signature from sorted bulk microglia, characterize its expression in bulk brain RNAseq across 7 datasets comprising 6 regions, in bulk fresh brain RNAseq and in microglial scRNAseq subtype clusters. This signature provides a well-characterized resource which can be utilized in analytic deconvolution studies of bulk transcriptome data^{33,34}. We uncovered microglial gene expression modules associated with age, sex and/or *APOE-ε4*. Modules with age and *APOE-ε4* associated transcriptional changes implicate microglial lipid and carbohydrate metabolism perturbations and microglial activation. Microglial scRNAseq data highlight the transcriptional complexity of this cell type, reveal both known and novel cell types and demonstrate utility of this data in characterizing sorted bulk RNAseq data. These findings provide support for the emerging microglial immunometabolism^{36,39} pathway as a plausible therapeutic target in aging-related disorders; and provide a well-characterized human transcriptome resource for the research community on this cell type with central roles in health and disease¹.

Methods

Patient Samples

Fresh human brain tissue was obtained from patients undergoing neurosurgical procedures for epilepsy or tumor resection. Tissues determined to be grossly unaffected by the primary disease process were utilized for the present study (**Supplementary Fig. 1**). Patient samples were transported from the operating room to the laboratory in 1X DPBS (ThermoFisher; 14287080) for processing within 1–2 hours of resection. Human tissue was collected with informed consent prior to surgery and all procedures were approved by the Mayo Clinic Institutional Review Board and are HIPAA compliant.

Tissue Dissociation

Tissue was dissected to remove necrotic tissue, white matter and excess vascular tissue, to retain only cortical grey matter. The remaining tissue was cut into sagittal slices and weighed before being processed using the Adult Brain Dissociation Kit (Miltenyi; 130-107-677) as per the manufacturer's protocol. Debris removal (Miltenyi; 130-109-398) and red blood cell lysis (Miltenyi; 130-094-183) were also performed. All procedures were carried out on ice. The resulting homogenate was filtered through a 70µm filter before proceeding.

Magnetic-Activated Cell Sorting (MACS)

The cell suspension was incubated with anti-CD11b microbeads (Miltenyi; 130-049-601 clone M1/70) for 15 minutes according to manufacturer's recommendation. This was then washed with PB buffer (0.5% BSA, 1X PBS Ca²⁺/Mg²⁺ free pH 7.4) and filtered through a 70µm cell strainer before being applied to a large separation column (Miltenyi; 130-042-401) in a QuadroMACS separator magnet (Miltenyi; 130-090-976). The CD11b⁺ fraction was collected and resuspended in sterile filtered FACS staining buffer (1X PBS Ca²⁺/Mg²⁺ free, 0.5% BSA, 2% FBS, 3mM EDTA) for antibody staining.

Fluorescence-Activated Cell Sorting (FACS)

The CD11b⁺ fraction was incubated in Human TruStain FcX blocking solution (1:20, Biolegend; 422302) at room temperature for 10 minutes. Subsequently, cells were stained with anti-CD11b PE/Cy7 (1:100, Biolegend; 101206, M1/70) and anti-CD45 Alexa Fluor 647 (1:100, Biolegend; 304056, HI30) antibodies for 30 minutes on ice. Following two washes with FACS staining buffer, SYTOX Green viability dye (1:1000, ThermoFisher; S7020) was added for an additional 20 minutes. Single cell suspensions were filtered through a 40µm cell strainer (Falcon; 352235) before sorting on a BD FACS Aria II (BD Biosciences). CD11b⁺/CD45^{intermediate}/SYTOX green⁻ cells were sorted directly into FACS staining buffer. An example of our FACS gating strategy is provided in **Supplementary Figure S2a**.

RNA Isolation and Sequencing

RNA from sorted microglial cells was isolated using the miRNeasy Serum/Plasma Kit (QIAGEN; 217184) and quantified on the Agilent BioAnalyzer 2100. cDNA libraries were generated using SMARTSeq2 v4 and

Nextera Low Input Library Prep Kit. Samples were multiplexed and sequenced on the Illumina HiSeq 4000.

RNA from frozen bulk tissue was isolated using Trizol and chloroform, followed by DNase and clean up using the RNeasy Kit (QIAGEN; 74106). Libraries were generated using the TruSeq Stranded mRNA Library Prep Kit. Samples were multiplexed and sequenced on the Illumina HiSeq 4000. Base-calling of all sequence data was performed using Illumina's RTA v2.7.7.

10X Single Cell 3' v3 Library Preparation of Sorted Microglia

Viability of MACS plus FACS sorted cells was assessed by Trypan blue (Gibco; 15250061) exclusion and cell density was determined using a hemocytometer prior to adjustment to target 4000–5000 cells. Cells were loaded onto a 10X Chromium chip and run on the GemCode Single Cell Instrument (10X Genomics) to generate single cell gel beads-in-emulsion (GEMs). Single cell RNA-seq libraries were prepared using the Chromium Single Cell 3' Gel Bead and Library Kit v2 and v3 (10X Genomics; 120237) and the Chromium i7 Multiplex Kit (10X Genomics; 120262) according to the manufacturer's instructions. Quality of cDNA libraries was determined using a BioAnalyzer 2100 DNA High Sensitivity assay (Agilent; 5067 – 4626) prior to sequencing one per lane on an Illumina HiSeq 4000.

Validation with Quantitative Real-Time PCR

Total RNA was extracted from sorted cells using the miRNeasy Serum/Plasma Kit (QIAGEN; 217184). Concentration and quality were assessed using the Agilent BioAnalyzer RNA 6000 Pico Kit (Agilent; 5067 – 1514). RNA was normalized to 0.5ng/μl for cDNA synthesis using the SuperScript IV VILO Master Mix (ThermoFisher; 11756050). TaqMan PreAmp Master Mix (ThermoFisher; 4391128) was used to pre-amplify the cDNA, followed by TaqMan Universal PCR Master Mix (ThermoFisher; 4304437) with the following gene expression probes: *MOG*, *AQP4*, *THY1*, *PTPRC*, *ITGAM*, *P2RY12*, *PECAM1*, *CD34*, *GAPDH* (ThermoFisher; Hs01555268_m1, Hs00242342_m1, Hs00174816_m1, Hs04189704_m1, Hs00355885_m1, Hs00224470_m1, Hs01065279_m1, Hs02576480_m1, Hs99999905_m1). RT-qPCR was performed on a QuantStudio 7 Flex Real-Time PCR System (ThermoFisher) using a relative standard curve to quantify gene expression.

Validation with Immunocytochemistry

Cultured cells were fixed with 4% paraformaldehyde (PFA) overnight at 4°C and blocked with blocking solution (10% BSA, 5% normal goat serum and 0.1% Triton-X). Fixed cells were stained with anti-TMEM119 (1:100, Biolegend; 853302) extracellular primary antibody with Goat anti-mouse IgG secondary antibody conjugated to Alexa-488 (1:100, Abcam; ab150113). Nuclei were stained with 1μg/ml DAPI (1:1000, ThermoFisher; 62248) before mounting with AquaPoly Mount (Poly Sciences, 18606-20). Images were acquired with a Zeiss LSM880 Confocal microscope using a Plan-Apochromat 20x magnification and 0.8 objective at 1024 by 1024 pixels with a 0.5 microsecond pixel dwell time.

Data Analysis

Bulk Microglia RNA-seq Processing

The MAPR-Seq pipeline²¹ was used to align reads to human reference genome hg38 using STAR²² and count reads using featureCounts²³. FastQC was used for quality control (QC) of raw sequence reads, and RSeQC was used for QC of mapped reads. Quality measures were examined including base calling quality, GC content, mapping statistics and sex check to ensure consistency between the recorded and inferred sex from expression of chromosome Y genes. Raw read counts were normalized using Conditional Quantile Normalization (CQN) to generate \log_2 scaled expression values via the Bioconductor package cqn, accounting for sequencing depth, gene length and GC content. Normalized CQN expression values were assessed using Principal components analysis (PCA) to identify and remove outliers, defined as greater than 4 standard deviations from the mean of the first two principal components. In addition, RPKM (reads per kilo bases per million) values were calculated.

Identification of a Core Microglial Signature from Bulk Microglia Data

To define a core microglial signature, we compared our bulk microglia data to AMP-AD bulk tissue transcriptome data from 7 different datasets representing 6 brain regions (Synapse ID: syn2580853); Mayo Clinic²⁴ (cerebellum and superior temporal gyrus), Mount Sinai Brain Bank²⁵ BM10 (frontal pole), BM22 (superior temporal gyrus), BM36 (parahippocampal gyrus), BM44 (inferior frontal gyrus) and Rush University Religious Order Study-Memory and Aging Project (ROS-MAP)²⁶ (dorsolateral prefrontal cortex). Raw gene counts and metadata (see Acknowledgements) were obtained from the AMP-AD RNAseq Harmonization study which had performed alignment and processing of all datasets and brain regions through a consensus pipeline²⁷. Samples were removed that had inconsistent sex between that indicated in metadata and that inferred from RNAseq expression; a RIN < 5; were identified as gene expression outliers based on principal component analysis (PCA) (> 4 standard deviation (SD) from mean PC1 or PC2), or missing metadata. In addition, duplicates (lowest read count sample removed) and those with rRNA (> 5%) were removed from the MSBB datasets. Furthermore, samples not meeting neuropathological criteria as Alzheimer's disease (AD)²⁸ or control were excluded. Raw read counts were normalized using Conditional Quantile Normalization (CQN). \log_2 fold change and q-values between each bulk tissue brain region and the bulk microglia profiles were calculated for each gene via linear regression using $\log_2(\text{RPKM})$ without correction for covariates. Genes were filtered using a cutoff of 4-fold greater expression in bulk microglia compared to each bulk tissue region and $q < 0.05$. Genes that passed these criteria and were significant in comparisons with all 7 bulk brain datasets determined the microglial signature. These signature genes were assessed for GO term enrichment with biological pathways using MSigDB. REViGO²⁹ tree plots were generated in R using GO terms obtained from MSigDB.

Weighted Gene Co-Expression Network Analysis

The CQN normalized expression values from bulk microglia were input to R WGCNA³⁰ package v1.69. This analysis included 14,149 expressed genes, i.e. median(CQN) > 2. Modules were identified, their

eigengenes were calculated and merged if correlation of eigengenes > 0.7 . Genes in the 40 modules identified were tested for GO term enrichment via WGCNA. Module membership (MM) for each gene was calculated as the correlation between expression of each gene and its module eigengene. Genes with $MM \geq 0.7$ are considered the hub genes for the network. Gene co-expression network plots were generated in Cytoscape v3.8 (<http://www.cytoscape.org/>). Each module eigengene was tested for association with age, sex and *APOE* using Pearson correlation. Co-expression network genes were annotated if they were significantly associated ($p < 0.05$) with the tested trait.

Over-Representation and Correlation Analyses

Hypergeometric testing was performed in R to determine the enrichment of a select set of genes in previously reported signatures, bulk tissue expressed genes, WGCNA modules or 10X single cell clusters. Correlation between bulk tissue and bulk microglial normalized CQN data was calculated using Spearman's rank correlation. Concordant and discordantly correlated genes were determined using the upper and lower quartiles from each dataset.

Single Cell Data Analysis

For single cell RNA samples, 10X Genomics Cell Ranger Single Cell Software Suite v3.1.0³¹ was used to demultiplex raw base call files generated from the sequencer into FASTQ files. Raw reads were aligned to human genome build GRCh38. Reads aligned to gene transcript locus were counted to generate raw UMI counts per gene per barcode for each sample. The raw UMI matrices were filtered to only keep barcodes with > 500 UMIs and those that were called a cell by Cell Ranger's cell calling algorithm.

Quality control, normalization, clustering and marker gene identification were performed with Seurat v3³², followed by annotation of clusters using established cell type markers. We kept 1) barcodes with $> 10\%$ of UMI mapped to mitochondrial genome; 2) barcodes with < 400 or > 8000 detected genes; 3) barcodes with < 500 or $> 46,425$ mapped UMIs; 4) genes that are detected in < 5 cells. These thresholds were determined by UMI or gene distribution to identify undetectable genes and outlier barcodes that may encode background, damaged or multiple cells. UMI counts of remaining cells and genes were normalized using NormalizeData function, which gave natural log transformed expression adjusted for total UMI counts in each cell. The top 2000 genes whose normalized expression varied the most across cells were identified through FindVariableFeatures function with default parameters. Using those genes, cells from 6 samples were integrated using functions FindIntegrationAnchors and IntegrateData with default parameters. Principal components (PCs) of the integrated and scaled data were computed; and the first 31 PCs, which accounted for $> 95\%$ variance, were used in clustering cells. Cell clustering was performed using FindNeighbors and FindClusters with default parameters. Marker genes were identified in each cluster using FindMarkers in Seurat. Marker genes on one cluster must 1) be present in $> 20\%$ cells in the cluster; 2) the $\log(\text{fold change})$ between expression in the cluster and other clusters must be > 0.25 ; 3) the rank sum test p-value (Bonferroni-adjusted) between cells in the cluster and cells in other clusters < 0.05 .

Abbreviations

AD: Alzheimer's disease

APOE: Apolipoprotein E

BM: Brodmann's area

BSA: Bovine serum albumin

CERAD: Consortium to Establish a Registry for Alzheimer's Disease

CNS: Central nervous system

CQN: Conditional quantile normalization

DAM: Disease-associated microglia

DPBS: Dulbecco's phosphate buffered saline

FACS: Fluorescence-activated cell sorting

FPKM: Fragments per kilobase of transcript per million mapped reads

GEM: Gel bead-in emulsion

GO: Gene ontology

MACS: Magnetic-activated cell sorting

ME: Module eigengenes

MM: Module membership

PBS: Phosphate buffered saline

PC: Principal component

PCA: Principle component analysis

PFA: Paraformaldehyde

QC: Quality control

RNAseq: RNA sequencing

ROSMAP: Rush University Religious Order Study-Memory and Aging Project

scRNAseq: Single cell RNA sequencing

snRNAseq: Single nuclei RNA sequencing

UMI: Unique molecular identifier

WGCNA: Weighted gene co-expression network analysis

Declarations

Data Sharing Statement

The data in this manuscript are available via the AD Knowledge Portal (<https://adknowledgeportal.synapse.org>). The AD Knowledge Portal is a platform for accessing data, analyses and tools generated by the Accelerating Medicines Partnership (AMP-AD) Target Discovery Program and other National Institute on Aging (NIA)-supported programs to enable open-science practices and accelerate translational learning. The data, analyses and tools are shared early in the research cycle without a publication embargo on secondary use. Data is available for general research use according to the following requirements for data access and data attribution (<https://adknowledgeportal.synapse.org/DataAccess/Instructions>).

Dataset	Data Type	Description	SynapseID	DoD
Mayo RNAseq TCX	Metadata	Individual human and RNAseq	syn5550404	na
Mayo RNAseq CER	Metadata	Individual human and RNAseq	syn5550404	na
Mayo RNAseq TCX	RNASeq Expression	Consensus processed RNASeq raw counts	syn8690799	10/2/2019
Mayo RNAseq CER	RNASeq Expression	Consensus processed RNASeq raw counts	syn8690904	10/2/2019
ROSMAP	Metadata	ID Key	syn3382527	10/2/2019
ROSMAP	Metadata	Individual human	syn3191087	10/2/2019
ROSMAP	Metadata	Assay RNAseq	syn21088596	1/2/2020
ROSMAP	RNASeq Expression	Consensus processed RNASeq raw counts	syn8691134	10/2/2019
MSBB	Metadata	Individual human	syn6101474	11/22/2019
MSBB	Metadata	Assay RNAseq	syn6100548	10/2/2019
MSBB	RNASeq Expression	Consensus processed RNASeq raw counts	syn8691099	10/2/2019

Data from AD knowledge portal utilized in this study. DoD = Date of download, “na” indicates data that was generated by study authors and shared within the AD knowledge portal. Data were obtained from the RNAseq Harmonization Study in the AD knowledge portal (DOI: <https://doi.org/10.7303/syn9702085>).

Author Contributions

TP and NET wrote the manuscript; NET and MA designed the study; TP, XW and ZQ performed data analysis; JC consulted on statistical methods; TP, TPC, XW, YM, RMA generated tables and figures; EM, CAG, SG, KC, RW, HGC and AQH provided neurosurgical tissue samples; TP, TPC, LJLT, SJL, SL, FQTN, CCGH, KGM, and TN performed experimental procedures from blood and tissue samples. All authors read the manuscript and provided input and consultation. NET oversaw the study and provided direction, funding and resources.

Competing Financial Interests

None

References

1. Masuda, T., Sankowski, R., Staszewski, O. & Prinz, M. Microglia heterogeneity in the single-cell era. *Cell Reports* **30**, 1271-1281 (2020).
2. Li, Q. & Barres, B.A. Microglia and macrophages in brain homeostasis and disease. *Nat Rev Immunol* **18**, 225-242 (2018).
3. Hickman, S., Izzy, S., Sen, P., Morsett, L. & El Khoury, J. Microglia in neurodegeneration. *Nat Neurosci* **21**, 1359-1369 (2018).
4. Keren-Shaul, H., *et al.* A unique microglia type associated with restricting development of Alzheimer's disease. *Cell* **169**, 1276-1290 e1217 (2017).
5. Krasemann, S., *et al.* The TREM2-APOE Pathway Drives the Transcriptional Phenotype of Dysfunctional Microglia in Neurodegenerative Diseases. *Immunity* **47**, 566-581 e569 (2017).
6. Mathys, H., *et al.* Single-cell transcriptomic analysis of Alzheimer's disease. *Nature* **570**, 332-337 (2019).
7. Del-Aguila, J.L., *et al.* A single-nuclei RNA sequencing study of Mendelian and sporadic AD in the human brain. *Alzheimer's Research & Therapy* **11**, 71 (2019).
8. Thrupp, N., *et al.* Single-nucleus RNA-seq is not suitable for detection of microglial activation genes in humans. *Cell Reports* **32**, 108189 (2020).
9. Olah, M., *et al.* Single cell RNA sequencing of human microglia uncovers a subset associated with Alzheimer's disease. *Nat Commun* **11**, 6129 (2020).

10. Masuda, T., *et al.* Spatial and temporal heterogeneity of mouse and human microglia at single-cell resolution. *Nature* **566**, 388-392 (2019).
11. Sankowski, R., *et al.* Mapping microglia states in the human brain through the integration of high-dimensional techniques. *Nat Neurosci* **22**, 2098-2110 (2019).
12. Galatro, T.F., *et al.* Transcriptomic analysis of purified human cortical microglia reveals age-associated changes. *Nat Neurosci* **20**, 1162-1171 (2017).
13. Olah, M., *et al.* A transcriptomic atlas of aged human microglia. *Nature Communications* **9**, 539 (2018).
14. Frigerio, C., *et al.* The major risk factors for Alzheimer's Disease: Age, sex, and genes modulate the microglia response to amyloid-beta plaques. *Cell Reports* **27**, 1293-1306 e1296 (2019).
15. Stephen, T.L., *et al.* APOE genotype and sex affect microglial interactions with plaques in Alzheimer's disease mice. *Acta Neuropathol Commun* **7**, 82 (2019).
16. Nelson, L.H., Warden, S. & Lenz, K.M. Sex differences in microglial phagocytosis in the neonatal hippocampus. *Brain, Behavior, and Immunity* **64**, 11-22 (2017).
17. Yamazaki, Y., Zhao, N., Caulfield, T.R., Liu, C.C. & Bu, G. Apolipoprotein E and Alzheimer disease: pathobiology and targeting strategies. *Nat Rev Neurol* **15**, 501-518 (2019).
18. Hammond, T.R., *et al.* Single-cell RNA sequencing of microglia throughout the mouse lifespan and in the injured brain reveals complex cell-state changes. *Immunity* **50**, 253-271 e256 (2019).
19. Grubman, A., *et al.* A single-cell atlas of entorhinal cortex from individuals with Alzheimer's disease reveals cell-type-specific gene expression regulation. *Nat Neurosci* **22**, 2087-2097 (2019).
20. Gamache, J., Yun, Y. & Chiba-Falek, O. Sex-dependent effect of APOE on Alzheimer's disease and other age-related neurodegenerative disorders. *Disease Models & Mechanisms* **13**, dmm045211 (2020).
21. Kalari, K.R., *et al.* MAP-RSeq: Mayo Analysis Pipeline for RNA sequencing. *BMC Bioinformatics* **15**, 224 (2014).
22. Dobin, A., *et al.* STAR: ultrafast universal RNA-seq aligner. *Bioinformatics* **29**, 15-21 (2013).
23. Liao, Y., Smyth, G.K. & Shi, W. featureCounts: an efficient general purpose program for assigning sequence reads to genomic features. *Bioinformatics* **30**, 923-930 (2014).
24. Allen, M., *et al.* Human whole genome genotype and transcriptome data for Alzheimer's and other neurodegenerative diseases. *Sci Data* **3**, 160089 (2016).
25. Wang, M., *et al.* The Mount Sinai cohort of large-scale genomic, transcriptomic and proteomic data in Alzheimer's disease. *Sci Data* **5**, 180185 (2018).
26. De Jager, P.L., *et al.* A multi-omic atlas of the human frontal cortex for aging and Alzheimer's disease research. *Sci Data* **5**, 180142 (2018).
27. Wan, Y.W., *et al.* Meta-Analysis of the Alzheimer's Disease Human Brain Transcriptome and Functional Dissection in Mouse Models. *Cell Rep* **32**, 107908 (2020).

28. McKhann, G., *et al.* Clinical diagnosis of Alzheimer's disease: report of the NINCDS-ADRDA Work Group under the auspices of Department of Health and Human Services Task Force on Alzheimer's Disease. *Neurology* **34**, 939-944 (1984).
29. Supek, F., Bosnjak, M., Skunca, N. & Smuc, T. REVIGO summarizes and visualizes long lists of gene ontology terms. *PLoS One* **6**, e21800 (2011).
30. Langfelder, P. & Horvath, S. WGCNA: an R package for weighted correlation network analysis. *BMC Bioinformatics* **9**, 559 (2008).
31. Zheng, G.X.Y., *et al.* Massively parallel digital transcriptional profiling of single cells. *Nature Communications* **8**, 14049 (2017).
32. Stuart, T., *et al.* Comprehensive Integration of Single-Cell Data. *Cell* **177**, 1888-1902.e1821 (2019).
33. McKenzie, A.T., *et al.* Brain Cell Type Specific Gene Expression and Co-expression Network Architectures. *Sci Rep* **8**, 8868 (2018).
34. Wang, X., *et al.* Deciphering cellular transcriptional alterations in Alzheimer's disease brains. *Mol Neurodegener* **15**, 38 (2020).
35. Gosselin, D., *et al.* An environment-dependent transcriptional network specifies human microglia identity. *Science* **356**(2017).
36. Chausse, B., Kakimoto, P.A. & Kann, O. Microglia and lipids: how metabolism controls brain innate immunity. *Semin Cell Dev Biol* (2020).
37. Loving, B.A. & Bruce, K.D. Lipid and Lipoprotein Metabolism in Microglia. *Front Physiol* **11**, 393 (2020).
38. Marschallinger, J., *et al.* Lipid-droplet-accumulating microglia represent a dysfunctional and proinflammatory state in the aging brain. *Nat Neurosci* (2020).
39. Bernier, L.P., York, E.M. & MacVicar, B.A. Immunometabolism in the Brain: How Metabolism Shapes Microglial Function. *Trends Neurosci* **43**, 854-869 (2020).
40. El Khoury, J., Hickman, S.E., Thomas, C.A., Loike, J.D. & Silverstein, S.C. Microglia, scavenger receptors, and the pathogenesis of Alzheimer's disease. *Neurobiol Aging* **19**, S81-84 (1998).
41. DePaula-Silva, A.B., *et al.* Differential transcriptional profiles identify microglial- and macrophage-specific gene markers expressed during virus-induced neuroinflammation. *J Neuroinflammation* **16**, 152-152 (2019).
42. Butovsky, O. & Weiner, H.L. Microglial signatures and their role in health and disease. *Nature Reviews Neuroscience* **19**, 622-635 (2018).
43. Colombo, A., *et al.* Loss of NPC1 enhances phagocytic uptake and impairs lipid trafficking in microglia. *Nature Communications* **12**, 1158 (2021).
44. Mehra, A., Ali, C., Parcq, J., Vivien, D. & Docagne, F. The plasminogen activation system in neuroinflammation. *Biochimica et Biophysica Acta (BBA) - Molecular Basis of Disease* **1862**, 395-402 (2016).

45. Cunningham, O., *et al.* Microglia and the urokinase plasminogen activator receptor/uPA system in innate brain inflammation. *Glia* **57**, 1802-1814 (2009).
46. Sobue, A., *et al.* Microglial gene signature reveals loss of homeostatic microglia associated with neurodegeneration of Alzheimer's disease. *Acta Neuropathologica Communications* **9**, 1 (2021).
47. Rangaraju, S., *et al.* Identification and therapeutic modulation of a pro-inflammatory subset of disease-associated-microglia in Alzheimer's disease. *Mol Neurodegener* **13**, 24 (2018).
48. Rangaraju, S., *et al.* Quantitative proteomics of acutely-isolated mouse microglia identifies novel immune Alzheimer's disease-related proteins. *Mol Neurodegener* **13**, 34 (2018).
49. Gerrits, E., *et al.* Distinct amyloid- β and tau-associated microglia profiles in Alzheimer's disease. *Acta Neuropathologica* **141**, 681-696 (2021).
50. Cermak, S., *et al.* Loss of Cathepsin B and L Leads to Lysosomal Dysfunction, NPC-Like Cholesterol Sequestration and Accumulation of the Key Alzheimer's Proteins. *PLOS ONE* **11**, e0167428 (2016).
51. Xu, H., Han, Y., Liu, B. & Li, R. Unc-5 homolog B (UNC5B) is one of the key downstream targets of N- α -Acetyltransferase 10 (Naa10). *Scientific Reports* **6**, 38508 (2016).
52. Ahn, E.H., Kang, S.S., Qi, Q., Liu, X. & Ye, K. Netrin1 deficiency activates MST1 via UNC5B receptor, promoting dopaminergic apoptosis in Parkinson's disease. *Proceedings of the National Academy of Sciences* **117**, 24503-24513 (2020).
53. Zhang, X., *et al.* A rare missense variant of CASP7 is associated with familial late-onset Alzheimer's disease. *Alzheimers Dement* **15**, 441-452 (2019).
54. Ayers, K.L., *et al.* A loss of function variant in CASP7 protects against Alzheimer's disease in homozygous APOE ϵ 4 allele carriers. *BMC Genomics* **17 Suppl 2**, 445 (2016).
55. Katsouri, L. & Georgopoulos, S. Lack of LDL receptor enhances amyloid deposition and decreases glial response in an Alzheimer's disease mouse model. *PLoS One* **6**, e21880 (2011).
56. Lämsä, R., *et al.* Genetic study evaluating LDLR polymorphisms and Alzheimer's disease. *Neurobiol Aging* **29**, 848-855 (2008).
57. Crotti, A., *et al.* BIN1 favors the spreading of Tau via extracellular vesicles. *Scientific Reports* **9**, 9477 (2019).
58. Sims, R., *et al.* Rare coding variants in PLCG2, ABI3, and TREM2 implicate microglial-mediated innate immunity in Alzheimer's disease. *Nature Genetics* **49**, 1373-1384 (2017).
59. Darmanis, S., *et al.* A survey of human brain transcriptome diversity at the single cell level. *Proceedings of the National Academy of Sciences* **112**, 7285 (2015).
60. Zhou, Y., *et al.* Human and mouse single-nucleus transcriptomics reveal TREM2-dependent and TREM2-independent cellular responses in Alzheimer's disease. *Nat Med* **26**, 131-142 (2020).
61. Schmunk, G., *et al.* Human microglia upregulate cytokine signatures and accelerate maturation of neural networks. *bioRxiv*, 2020.2003.2024.006874 (2020).
62. Aung, L.L., *et al.* Multiple sclerosis-linked and interferon-beta-regulated gene expression in plasmacytoid dendritic cells. *J Neuroimmunol* **250**, 99-105 (2012).

63. Satoh, J., *et al.* Microarray analysis identifies an aberrant expression of apoptosis and DNA damage-regulatory genes in multiple sclerosis. *Neurobiol Dis* **18**, 537-550 (2005).
64. Gandhi, K.S., *et al.* The multiple sclerosis whole blood mRNA transcriptome and genetic associations indicate dysregulation of specific T cell pathways in pathogenesis. *Hum Mol Genet* **19**, 2134-2143 (2010).
65. Allen, M., *et al.* Divergent brain gene expression patterns associate with distinct cell-specific tau neuropathology traits in progressive supranuclear palsy. *Acta Neuropathol* **136**, 709-727 (2018).
66. Allen, M., *et al.* Conserved brain myelination networks are altered in Alzheimer's and other neurodegenerative diseases. *Alzheimers Dement* **14**, 352-366 (2018).
67. Mostafavi, S., *et al.* A molecular network of the aging human brain provides insights into the pathology and cognitive decline of Alzheimer's disease. *Nat Neurosci* **21**, 811-819 (2018).
68. Neff, R.A., *et al.* Molecular subtyping of Alzheimer's disease using RNA sequencing data reveals novel mechanisms and targets. *Sci Adv* **7**(2021).
69. Alsema, A.M., *et al.* Profiling Microglia From Alzheimer's Disease Donors and Non-demented Elderly in Acute Human Postmortem Cortical Tissue. *Frontiers in Molecular Neuroscience* **13**(2020).
70. Srinivasan, K., *et al.* Alzheimer's Patient Microglia Exhibit Enhanced Aging and Unique Transcriptional Activation. *Cell Rep* **31**, 107843 (2020).
71. Shi, Y., *et al.* Microglia drive APOE-dependent neurodegeneration in a tauopathy mouse model. *Journal of Experimental Medicine* **216**, 2546-2561 (2019).
72. Nguyen, A.T., *et al.* APOE and TREM2 regulate amyloid-responsive microglia in Alzheimer's disease. *Acta Neuropathologica* **140**, 477-493 (2020).
73. Leduc, V., Jasmin-Belanger, S. & Poirier, J. APOE and cholesterol homeostasis in Alzheimer's disease. *Trends Mol Med* **16**, 469-477 (2010).
74. Paciotti, S., Albi, E., Parnetti, L. & Beccari, T. Lysosomal Ceramide Metabolism Disorders: Implications in Parkinson's Disease. *J Clin Med* **9**(2020).
75. Nugent, A.A., *et al.* TREM2 Regulates Microglial Cholesterol Metabolism upon Chronic Phagocytic Challenge. *Neuron* **105**, 837-854 e839 (2020).
76. Yeh, F.L., Wang, Y., Tom, I., Gonzalez, L.C. & Sheng, M. TREM2 Binds to Apolipoproteins, Including APOE and CLU/APOJ, and Thereby Facilitates Uptake of Amyloid-Beta by Microglia. *Neuron* **91**, 328-340 (2016).
77. Norden, D.M. & Godbout, J.P. Review: microglia of the aged brain: primed to be activated and resistant to regulation. *Neuropathol Appl Neurobiol* **39**, 19-34 (2013).
78. Koellhoffer, E.C., McCullough, L.D. & Ritzel, R.M. Old maids: Aging and its impact on microglia function. *Int J Mol Sci* **18**(2017).
79. Ulland, T.K., *et al.* TREM2 Maintains Microglial Metabolic Fitness in Alzheimer's Disease. *Cell* **170**, 649-663 e613 (2017).

80. Lin, Y.T., *et al.* APOE4 Causes Widespread Molecular and Cellular Alterations Associated with Alzheimer's Disease Phenotypes in Human iPSC-Derived Brain Cell Types. *Neuron* **98**, 1141-1154 e1147 (2018).
81. Andreone, B.J., *et al.* Alzheimer's-associated PLCgamma2 is a signaling node required for both TREM2 function and the inflammatory response in human microglia. *Nat Neurosci* **23**, 927-938 (2020).
82. Grassivaro, F., *et al.* Convergence between Microglia and Peripheral Macrophages Phenotype during Development and Neuroinflammation. *The Journal of Neuroscience* **40**, 784-795 (2020).
83. Chrétien, F., *et al.* Expression of Excitatory Amino Acid Transporter-1 (EAAT-1) in Brain Macrophages and Microglia of Patients with Prion Diseases. *Journal of Neuropathology & Experimental Neurology* **63**, 1058-1071 (2004).
84. Wilhelmsson, U., *et al.* Injury Leads to the Appearance of Cells with Characteristics of Both Microglia and Astrocytes in Mouse and Human Brain. *Cerebral Cortex* **27**, 3360-3377 (2017).

Figures

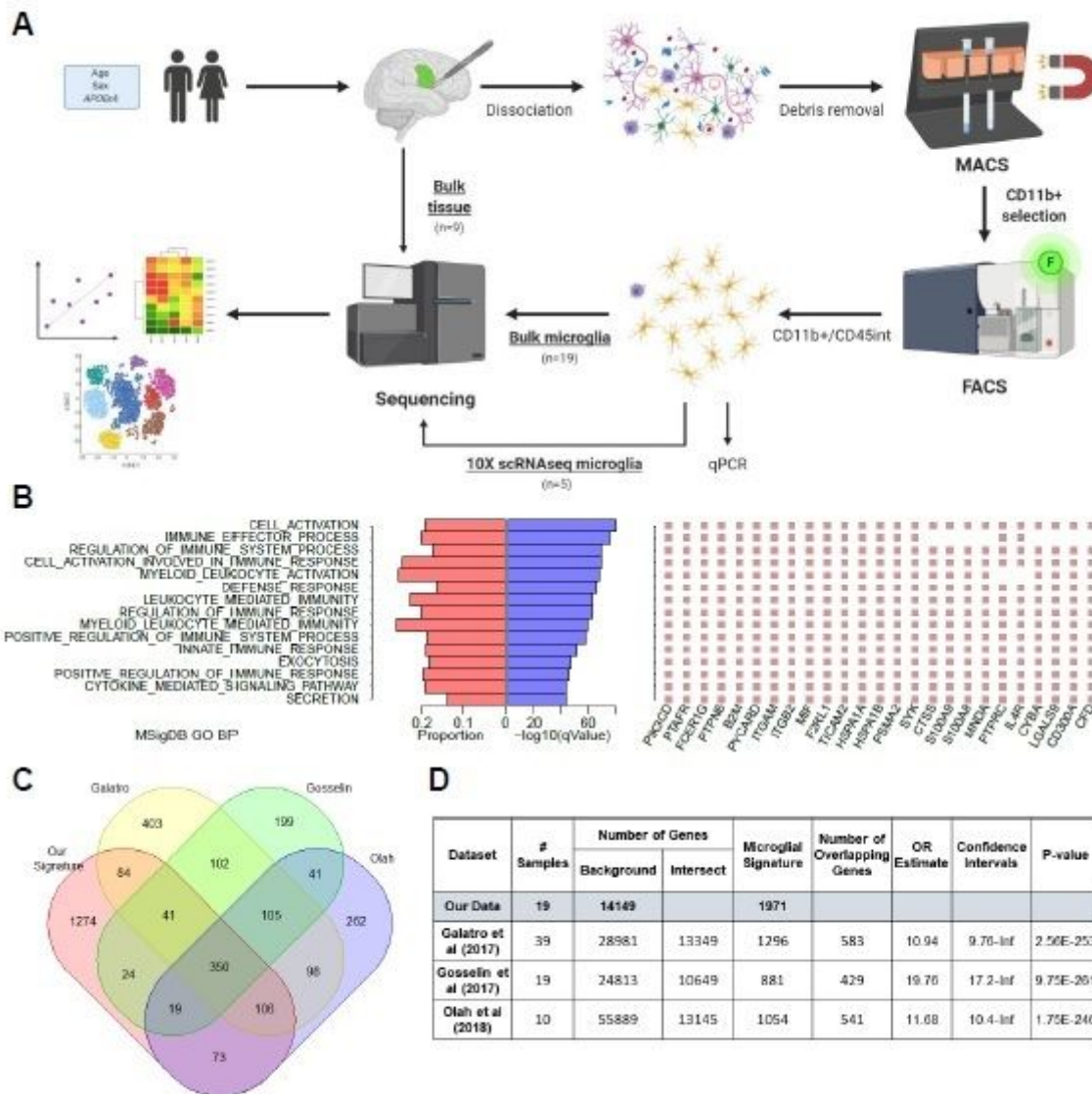


Figure 1

Characterization of our core human microglial signature. (A) Schematic illustrating our experimental approach for isolating microglial populations from fresh brain tissue and data analyses. [Created with BioRender.com] (B) MSigDB GO terms enriched in our microglial signature genes and top 25 genes for each. (C) Venn diagram showing number of overlapping genes between our microglial signature and those previously reported from Galatro et al (2017), Gosselin et al (2017) and Olah et al (2018). (D) Hypergeometric tests of overrepresentation showing overlap with the published signatures.

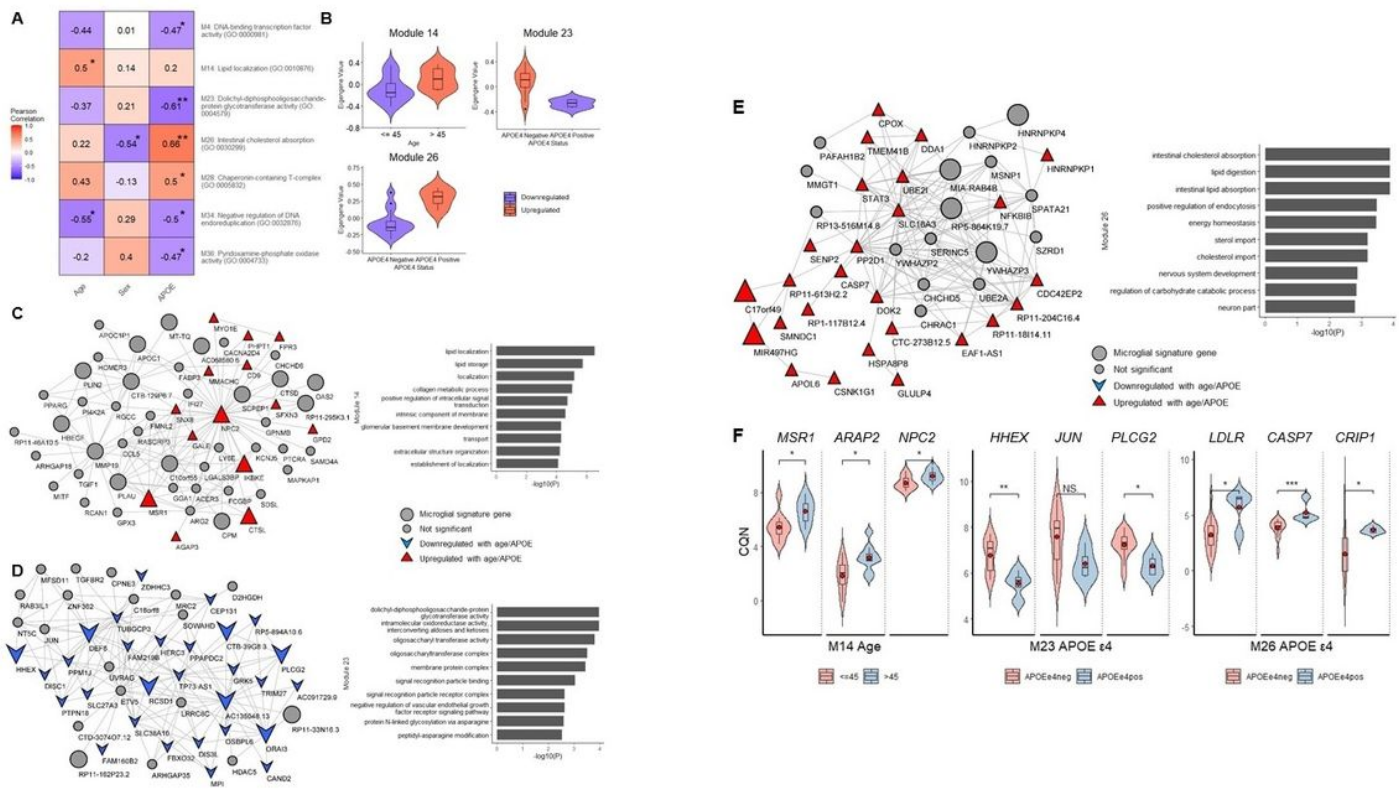


Figure 2

Age, sex and APOE ε4 pathway correlations in bulk microglia. (A) Heatmap showing correlation of age, sex and APOE ε4 status with WGCNA module eigengenes (MEs) significantly associated (* p < 0.05; ** p < 0.01 *** p < 0.001) with traits, with top GO terms listed for each module. (B) MEs stratified by age or APOE ε4. (c-e) Gene co-expression networks for modules of interest. Genes were tested for association with age, sex or APOE ε4 status using Pearson correlation. (C) Module 14 gene co-expression network, with genes of interest highlighted according to the key. Genes upregulated with age (p < 0.05) shown in red triangle (▲). Bar plot of top 10 significant GO terms (p < 0.05) for this module. (D) Module 23 gene co-expression network, with genes downregulated in APOE ε4 carriers (p < 0.05) shown in blue arrow (▼). Bar plot of top 10 significant GO terms (p < 0.05) for this module. (E) Module 26 gene co-expression network, with genes upregulated in APOE ε4 carriers (p < 0.05) shown in red triangle (▲). Bar plot of top 10 significant GO terms (p < 0.05) for this module. (F) Violin plots showing expression of key genes in modules, stratified by age or APOE. * p < 0.05; ** p < 0.01; *** p < 0.001.

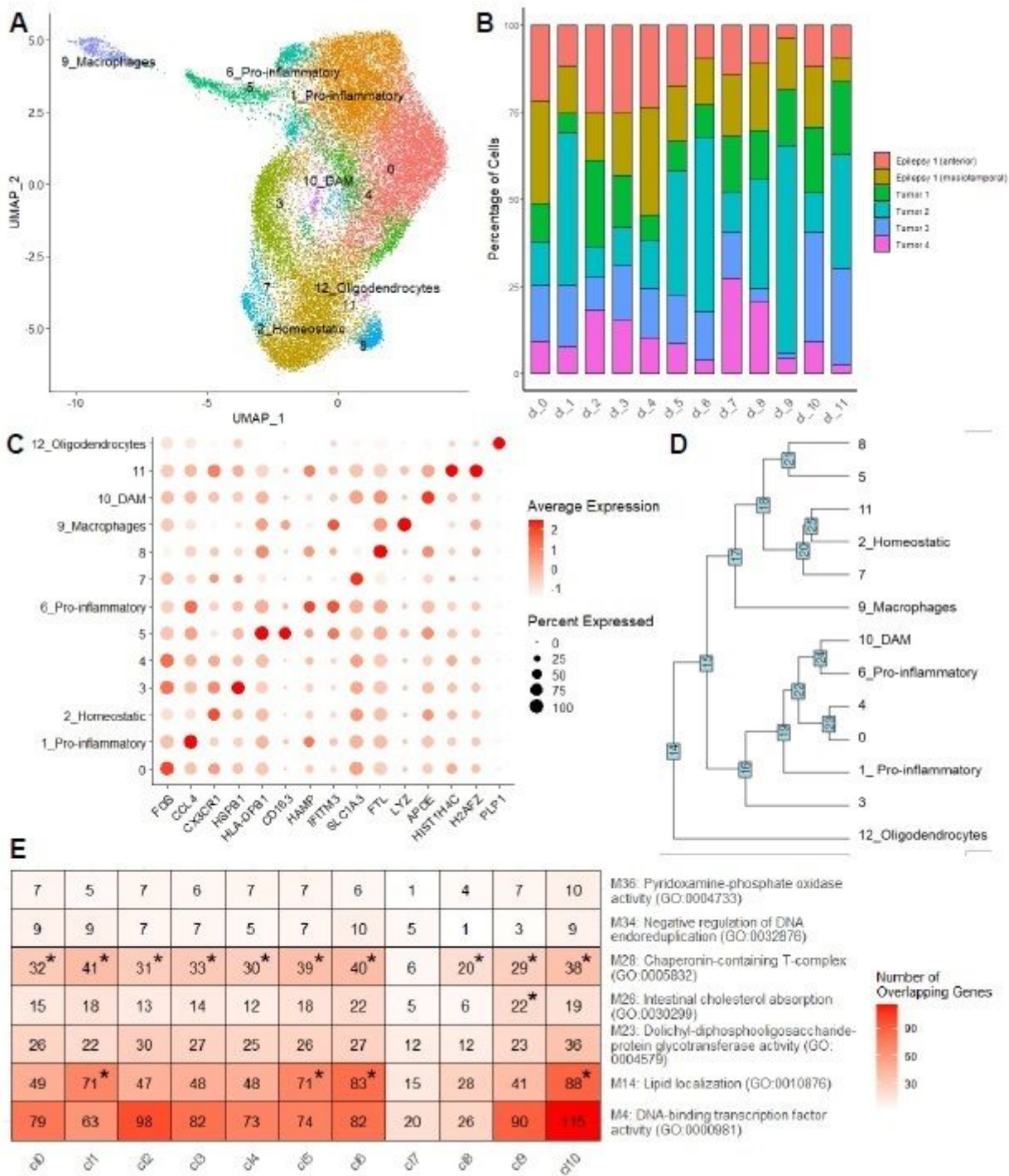


Figure 3

Single cell characterization of microglia. (A) UMAP of clustered cells annotated with putative subtypes using cell type markers from the literature. (B) Stacked bar plot showing the distribution of cells across the clusters. (C) Dot plot showing the expression of top cluster marker genes across clusters. (D) Hierarchical clustering to highlight relationships between clusters. (E) Hypergeometric distribution of enrichment between module genes and clusters, showing number of overlapping genes. * represents module genes that were significantly enriched in the cluster ($p < 0.05$).

Supplementary Files

This is a list of supplementary files associated with this preprint. Click to download.

- [MicrogliaSupplementaryFigures05122021.pdf](#)
- [MicrogliaSupplementaryTables05122021.xlsx](#)